THE ASTROPHYSICAL JOURNAL, 378:77–92, 1991 September 1

THE *EXOSAT* HIGH GALACTIC LATITUDE SURVEY[1]

P. GIOMMI,[2,3] G. TAGLIAFERRI,[2] K. BEUERMANN,[4,5] G. BRANDUARDI-RAYMONT,[6] R. BRISSENDEN,[7] U. GRASER,[8] K. O. MASON,[6] J. D. P. MITTAZ,[6] P. MURDIN,[9] G. POOLEY,[10] H.-C. THOMAS,[11] AND I. TUOHY[7]

Received 1990 November 30; accepted 1991 March 13

ABSTRACT

A survey of serendipitous sources performed in the very soft X-ray band (0.05–2.0 keV) using the *EXOSAT* imaging telescopes is presented. The survey covers 783 square degrees of high Galactic latitude sky and includes 210 serendipitous sources which define a complete (flux-limited) sample. An extensive program of optical and radio observations together with cross-correlations with catalogs of known objects leads to the identification of 200 of the 210 detected sources. The 10 remaining objects have been preliminarily classified on the basis of their X-ray to optical flux ratio, thus making the sample essentially fully identified. Twenty-three additional serendipitous sources that did not satisfy the requirements for inclusion in the complete sample were also identified during the optical observations program. The complete sample has been used to study the log N–log S relation and the average spectral slope of active galactic nuclei (AGN). It is found that the log N–log S slope is consistent with that of the *Einstein* Extended Medium-Sensitivity Survey (EMSS) and with the "Euclidean" value of 1.5. The normalization of the log N–log S relation is a strong function of the assumed spectral slope of AGNs. Consistency with the results of the EMSS implies that the average (energy) slope of extragalactic sources in the soft X-ray band is very steep ($\alpha \approx 1.5$). An analysis of the association between AGN detection and Galactic N_H also shows that α is steep and inconsistent with the canonical value of 0.7. The survey was particularly successful in detecting nearby Galactic soft X-ray emitters and includes a significantly higher percentage of stars than the *Einstein* EMSS, five white dwarfs and three previously unknown AM Herculis–type systems.

Subject headings: BL Lacertae objects — galaxies: nuclei — galaxies: X-rays — quasars — stars: X-rays — X-rays: sources

1. INTRODUCTION

Over the past few years, much effort has been dedicated to the search for serendipitous sources in *Einstein* imaging proportional counter (IPC) images and to the identification of their optical and radio counterparts (e.g., Maccacaro et al. 1982; Reichert et al. 1982; Stocke et al. 1983; Gioia et al. 1984; Margon, Downes, & Chanan 1985; Gioia et al. 1990). In some cases these sources have been used to construct well-defined flux-limited samples that are useful for studying the statistical properties of several types of cosmic X-ray emitters. Much of what is known about the log N–log S relation, the cosmological evolution, and the luminosity function of extragalactic sources in the X-ray band has been obtained from these data. Important information about the population of late-type stars was also obtained (e.g., Fleming et al. 1988; Fleming, Gioia, & Maccacaro 1989).

In this paper we present the results of a similar project carried out using data from the X-ray telescopes aboard *EXOSAT* (see Taylor et al. 1981 and White & Peacock 1989 for a description). These instruments were sensitive between 0.05 and 2.0 keV, an energy band very similar to that of the *ROSAT* X-ray telescope (Trümper 1983). A flux-limited and complete sample including 210 serendipitous sources has been constructed and has been used for the determination of the log N–log S relation of extragalactic sources, as well as for the investigation of the soft excess in AGNs, which seems to be a common and important phenomenon in this energy band (e.g., Arnaud et al. 1985; Wilkes & Elvis 1987; Turner & Pounds 1989; Kruper, Urry, & Canizares 1990). Results on the luminosity function and cosmological evolution of AGNs from this sample are presented in Giommi et al. (1991).

2. THE SURVEY

EXOSAT operated from 1983 May to 1986 April, and during this period 1780 observations were made. In the vast majority of cases the low-energy imaging telescope (LEIT-1)[12] with the channel multiplier array (CMA) detector (DeKorte et al. 1981) at its focus, was collecting data. More than three thousand X-ray images were obtained during the satellite life-

[1] Based on observations made with *EXOSAT*, with optical telescopes at Calar Alto, La Palma, and La Silla and with the Anglo-Australian Telescope, and with the radio telescopes at Cambridge, England, and Parkes, Australia.

[2] *EXOSAT* Observatory, Astrophysics Division, Space Science Department of ESA, Keplerlaan 1, 2200AG Noordwijk, The Netherlands.

[3] On leave of absence from Istituto di Fisica Cosmica del CNR, Milano, Italy.

[4] Institut für Astronomie und Astrophysik, Technische Universität, Hardenbergstrasse 36, 1000 Berlin, Germany.

[5] Max-Planck-Institut für Extraterrestrische Physik, Karl Schwarzschild Strasse 1, 8046 Garching bei München, Germany.

[6] Mullard Space Science Laboratory, University College London, Holmbury St Mary, Dorking, Surrey RH5 6NT, England.

[7] Australian National University, Private Bag, Weston Creek Post Office, ACT 2611, Australia.

[8] Max-Planck-Institut für Astronomie, Königstuhl, 6900 Heidelberg, Germany.

[9] Royal Greenwich Observatory, Madingley Road, Cambridge CB3 0EZ, England.

[10] Mullard Radio Astronomy Observatory, Madingley Road, Cambridge CB3 0EZ, England.

[11] Max-Planck-Institut für Astrophysik, Karl Schwarzschild Strasse 1, 8046 Garching bei München, Germany.

[12] The *EXOSAT Observatory* had on board two identical X-ray telescopes called LEIT-1 and LEIT-2, but only LEIT-1 operated throughout the mission.

time. All data have been reduced in a systematic and uniform way, and the results have been collected in a large computer-accessible data base (Giommi et al. 1988a; White & Giommi 1990). From this data base we have extracted a large set of X-ray images which have been subsequently searched for serendipitous sources. The set consists of 443 nonoverlapping CMA fields observed using the thin Lexan filter, which provided maximum photon throughput for most spectral shapes. The fields were selected using the following criteria: (*a*) observations were made using telescope LEIT-1 after 1983 August 10; (*b*) the pointing was at high Galactic latitude ($|b| > 20°$); and (*c*) exposure time was greater than 2000 s.

In addition, pointings of the Magellanic Clouds and of other crowded or confused areas (e.g., the Pleiades) were not considered.

When more than one image of the same area of sky was available, the one with the highest sensitivity was selected. Finally, a small area (about 3′ in size) centered on the target of the observation was excluded from the source search.

In the following this set of observations will be referred to as the *EXOSAT* High Galactic Latitude Survey (HGLS).

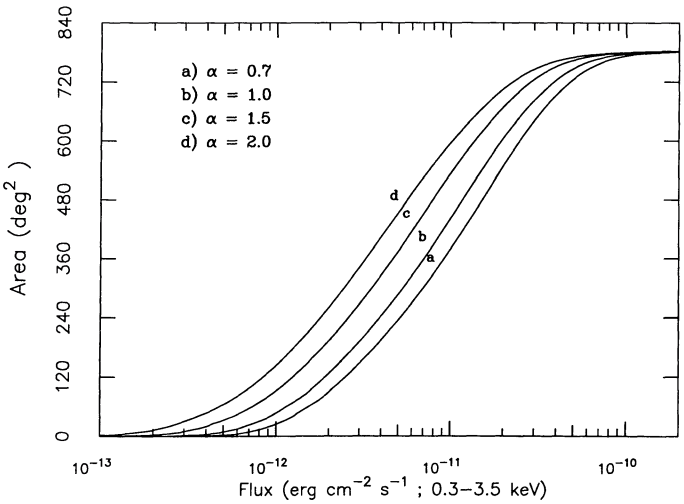

FIG. 1.—Sky coverage of the HGLS for different assumptions of the spectral index of extragalactic sources. Flux (*S*) is corrected for Galactic absorption and is calculated in the 0.3–3.5 keV band.

3. DATA ANALYSIS

All images of the *EXOSAT* HGLS have been searched for sources using a detect routine that locates excesses above the local background and that is optimized for the detection of point sources. In order to maximize sensitivity over the entire field of view, the size of the search cell was an increasing function of off-axis angle. This is necessary to compensate for the degradation of the point-spread function (PSF) at large off-axis angles (e.g., Giommi 1985). Since the software was optimized for the detection of point sources, the sensitivity to extended sources is poor and low surface brightness extended objects are likely to have been missed. All detections have been carefully reanalyzed using interactive software, and all excesses due to systematic features in the spatial structure of the CMA background have been removed. All mispointed targets were also removed.

4. THE SKY COVERAGE

The sky coverage of a survey is the relation that gives the area of sky surveyed at any given limiting sensitivity. Because of the wide range of exposure times, the different amounts of Galactic absorbing material (N_H) along the pointing direction of each field, and the strong variation of the sensitivity across the CMA field of view (Giommi 1985), the sky coverage of the HGLS is not a simple function of the number of images used.

The CMA limiting sensitivity, *S*, strongly changes within the image and can be expressed as a simple function of off-axis angle *r* (Giommi 1985):

$$S(r) = S_0 f(r) , \qquad (1)$$

where S_0 is the limiting sensitivity at image center, which is a function of exposure time and background level; $f(r)$ is a function of *r* only. Taking into account the calibration of the CMA (Giommi 1985; Giommi & Angelini 1987) and the threshold used to search for sources, $f(r)$ can be written as

$$f(r) = \begin{cases} 1.0 & \text{if } r \leq 12' , \\ 0.29 \times 10^{0.044r} & \text{if } 12 < r < 45' . \end{cases}$$

This sensitivity threshold is somewhat conservative but ensures that all sources with intensity greater than that of equation (1) are detected with a *statistical* signal-to-noise ratio of at least 4.[13] This minimizes the number of spurious detections and eliminates the need for a correction in the estimate of the log *N*–log *S* slope, which is necessary when sources detected just above the sensitivity limit are used (Maccacaro et al. 1982; Maccacoro, Romaine, & Schmitt 1986 and references therein). CMA images become background-limited for exposures longer than about 2000 s. Since the minimum exposure time in the 443 fields of the HGLS survey was chosen to be 2000 s, the photon-limited case in the above expression need not be considered.

The sky coverage of the HGLS for extragalactic pointlike sources whose spectrum is well approximated by a power-law model is shown in Figure 1, and has been calculated taking into account the above formulae and the amount of N_H in the direction of each pointing obtained from the 21 cm data of Stark et al. (1984) and from data collected with the Parkes radio telescope (see Giommi, Tagliaferri, & Angelini 1988b for details). Because of the fairly large bandpass of the *EXOSAT* CMA, the sky coverage depends strongly on the sources' spectral shape. This is shown in Figure 1 for a power-law spectrum with energy index α of 0.7, 1.0, 1.5, and 2.0. In order to facilitate a comparison with the *Einstein* EMSS, the limiting sensitivity is given in the 0.3–3.5 keV range and refers to flux (*S*) corrected for Galactic absorption.

5. THE SAMPLE

Using the procedure described above, 210 serendipitous sources were detected above the sensitivity limits used to construct the sky coverage of Figure 1. These sources make up a complete flux-limited sample that can be used for statistical analysis. Table 1 lists all sources in the sample. Column (1) gives the *EXOSAT* name; column (2) gives the celestial coordinates (for the 1950.0 equinox); column (3) gives an estimate of the 90% error radius in arcseconds calculated using the results of Osborne (1991) and taking into account that many sources

[13] The ratio between the count rate and the quoted errors of some of the sources listed in Table 1 is less than 4 because the errors given in the table include both statistical and systematic uncertainties.

TABLE 1

X-RAY, OPTICAL, AND RADIO DATA

Source Name (1)	Right Ascension Declination (1950.0) (2)	Error Radius (arcsec) (3)	N_H (10^{20}) z (4)	Count Rate (counts s^{-1}) (10^{-3}) (5)	m_v α_{ox} (6)	Radio Flux (mJy) α_{ro} (7)	Class Reference (8)	Comment (9)
EXO0003.4+2014	00 03 25.6	30	4.2	2.5	18.1	-	AGN	
	20 14 29		0.388	0.6	1.1		1	
EXO0007.4+1052	00 07 28.7	15	5.7	130.3	5.5	-	star	HD 560
	10 52 00		-	5.1	2.7		2	IPC
EXO0011.3-7457	00 11 23.0	65	4.8	36.0	12.0	-	star	IPC
	-74 57 33		-	6.0	1.9		3	
EXO0044.4+2001	00 44 29.9	30	3.4	1.1	18.0	61[a]	Class 1	see text
	20 01 22		-	0.3	1.3	0.5	1	
EXO0051.5+2507	00 51 35.5	30	5.0	4.8	8.2	-	star	HD 5237
	25 07 21		-	1.1	2.9		3	
EXO0100.0+3132	01 00 03.8	45	5.4	79.2	5.5	-	star	HD 6118
	31 32 12		-	9.9	2.8		3	
EXO0109.3-2613	01 09 19.6	30	1.7	3.2	8.8	-	star	SAO 166864
	-26 13 44		-	0.6	2.8		3	
EXO0111.4-1458	01 11 28.1	30	1.9	8.0	17.0	< 8[a]	AGN	
	-14 58 29		0.054	1.7	1.2		1	
EXO0117.2-2837	01 17 13.3	35	1.6	7.5	16.1	< 18[a]	AGN	IPC
	-28 37 27		0.351	1.5	1.4		1	
EXO0134.4+2026	01 34 24.6	15	4.9	13.4	8.7	-	star	IPC
	20 26 53		-	1.0	2.6		3	
EXO0146.5+0608	01 46 30.5	30	4.5	5.2	12.8[†]	-	star	
	06 08 53		-	1.4	2.1		3	
EXO0205.4+1454	02 05 29.0	25	6.0	10.9	14.4	< 6[b]	star	IPC
	14 54 23		-	1.5	1.8		1,4	
EXO0224.5+3045	02 24 30.6	20	7.4	37.5	10.1	-	star	IPC
	30 45 09		-	2.2	2.2		3	
EXO0232.1-0900	02 32 11.2	35	2.7	38.4	14.3	3[c]	AGN	HRI-IPC
	-09 00 16		0.043	3.8	1.3	0.0	3	MKN 1048
EXO0235.2-5216	02 35 12.0	15	3.3	15.7	12.1	-	star	
	-52 16 11		-	2.7	2.0		1	
EXO0237.1+0004	02 37 09.9	70	2.8	2470.8	4.1	-	star	HD 16582
	00 04 46		-	248.4	2.4		3	
EXO0244.8-0024	02 44 53.6	20	2.9	37.8	8.9	-	star	IPC
	-00 24 55		-	3.7	2.4		3	
EXO0313.4+3200	03 13 27.9	60	12.7	31.1	6.1	-	star	HD 20277
	32 00 33		-	5.2	2.9		3	
EXO0316.9+1853	03 16 56.5	15	9.6	11.7	7.4	-	star	HD 20629
	18 53 26		-	2.2	2.8		3	
EXO0329.9-2606	03 29 56.5	20	1.0	72.4	17.4	-	C.V.	AM Her type
	-26 06 58		-	6.3	1.0		5	
EXO0333.3-2554	03 33 19.7	45	1.0	466.3	18.6	< 4[a]	C.V.	AM Her type
	-25 54 10		-	32.1	0.5		6	
EXO0334.3+0014	03 34 19.0	15	7.3	4.5	4.3	-	star	HD 22484
	00 14 30		-	0.6	3.5		3	
EXO0336.3+0929	03 36 20.4	20	17.0	2.6	9.0	-	star	HD 22670
	09 29 37		-	0.5	2.8		3	
EXO0410.8+1005	04 10 49.8	15	13.3	50.5	6.2	-	star	HD 26676
	10 05 31		-	2.4	2.8		3	
EXO0411.8+1034	04 11 49.4	35	13.3	9.0	7.1	-	star	HD 26784
	10 34 03		-	1.7	2.9		3	
EXO0411.8+0953	04 11 51.3	35	13.3	174.1	5.2	-	star	HD 26793
	09 53 37		-	11.2	2.7		3	
EXO0412.4-0803	04 12 27.0	15	5.4	7.5	14.9	2[c]	AGN	HRI-IPC
	-08 03 02		0.037	1.5	1.4	0.0	3	
EXO0416.1-5505	04 16 6.6	20	1.8	7.4	15.4	< 5[a]	W.D.	
	-55 05 15		-	1.5	1.7		1	
EXO0419.0-5443	04 19 4.1	30	1.8	4.4	19.0	-	AGN	IPC
	-54 43 07		0.126	1.0	1.1		1	
EXO0419.2+1908	04 19 13.0	15	19.4	67.5	14.0	< 6[b]	star	IPC
	19 08 25		-	4.9	1.6		1	
EXO0429.1+0539	04 29 10.6	40	10.7	38.4	6.7	-	star	HD 28715
	05 39 06		-	4.6	2.7		3	
EXO0429.4+0518	04 29 25.0	30	10.7	12.0	6.4	-	star	HD 28736
	05 18 20		-	3.7	3.1		3	IPC

TABLE 1—*Continued*

Source Name (1)	Right Ascension Declination (1950.0) (2)	Error Radius (arcsec) (3)	N_H (10^{20}) z (4)	Count Rate (counts s^{-1}) (10^{-3}) (5)	m_v α_{ox} (6)	Radio Flux (mJy) α_{ro} (7)	Class Reference (8)	Comment (9)
EXO0430.5-1252	04 30 35.5	30	3.8	3.3	15.0	-	Gal	MCG02-12-0037
	-12 52 09		0.035	0.9	1.6		3	
EXO0431.4+0527	04 31 28.4	30	10.7	12.5	5.7	-	star	HD 28978
	05 27 50		-	3.7	3.1		3	
EXO0451.5-5547	04 51 30.3	15	1.9	102.3	7.8	-	star	HD 31407
	-55 47 03		-	5.5	2.4		3	
EXO0459.3+0132	04 59 22.4	60	7.3	97.7	7.9	-	star	SAO 112341
	01 32 29		-	13.4	2.4		3	
EXO0508.6-0414	05 08 39.0	30	9.5	28.7	9.3	-	star	HD 293857
	-04 14 18		-	7.6	2.4		3	
EXO0510.6-1615	05 10 41.2	35	5.8	879.7	3.3	-	star	HD 33904
	-16 15 41		-	55.2	2.7		3	IPC
EXO0512.8+0000	05 12 48.3	15	8.8	15.6	8.0	-	star	HD 34179
	00 00 10		-	3.1	2.7		3	
EXO0515.2-4557	05 15 15.7	40	2.7	19.1	7.0	-	star	HD 34631
	-45 57 30		-	2.9	2.8		3	
EXO0515.4-0005	05 15 27.0	35	11.0	76.1	7.4	-	star	HD 34511
	-00 05 15		-	5.7	2.6		3	
EXO0518.5-4547	05 18 32.7	30	2.7	2.4	19.0	-	Class 1	
	-45 47 44		-	0.7	1.1			
EXO0519.3-4544	05 19 22.3	30	2.7	4.0	11.9	-	star	IPC
	-45 44 22		-	1.0	2.3		9	
EXO0524.7-1155	05 24 43.8	70	10.2	146.5	6.3	-	star	HD 35850
	-11 55 40		-	16.3	2.6		3	
EXO0526.7-3301	05 26 47.4	30	2.3	1.9	18.7	$< 5^a$	AGN	IPC
	-33 01 21		1.236	0.5	1.2		9	
EXO0526.8-3328	05 27 00.0	60	2.3	21.9	12.0	-	star	
	-33 28 30		-	2.9	2.0		1	
EXO0527.1-3329	05 27 7.5	60	2.3	51.4	10.6	-	star	
	-33 29 15		-	5.6	2.1		1	
EXO0527.8-3241	05 27 52.7	30	1.8	2.3	13.7	-	star	IPC
	-32 41 38		-	0.7	2.1		1	
EXO0532.9-5819	05 32 59.7	30	3.6	2.4	19.5	-	Class 1	
	-58 19 37		-	0.7	1.0			
EXO0540.9-4046	05 40 54.6	15	3.3	2.5	13.0	-	star	
	-40 46 29		-	0.4	2.2		1	
EXO0541.0-4056	05 41 5.2	30	3.3	1.3	19.5	-	Class 1	
	-40 56 31		-	0.3	1.1			
EXO0541.7-4049	05 41 47.3	15	3.3	5.8	17.4	$< 6^a$	AGN	
	-40 49 48		0.099	0.6	1.1		1	
EXO0554.0-3806	05 54 2.5	30	3.6	14.6	7.6	-	star	HD 40216
	-38 06 42		-	2.5	2.8		3	
EXO0556.1-3804	05 56 9.2	15	3.6	40.7	9.7	-	star	
	-38 04 29		-	2.0	2.3		1	
EXO0556.4-3838	05 56 25.5	25	3.9	42.9	17.1	55^a	BL-Lac	
	-38 38 39		-	3.9	0.9	0.4	1	
EXO0557.9-5112	05 57 55.0	60	5.2	45.1	7.0	-	star	HD 40909
	-51 12 40		-	6.0	2.7		3	
EXO0615.1+8222	06 15 11.0	30	5.5	6.2	10.3	-	star	SAO 996
	82 22 56		-	1.4	2.5		3	
EXO0630.5+8218	06 30 36.0	30	5.2	11.7	9.8†	-	star	HD 44982
	82 18 38		-	2.5	2.6		3	
EXO0635.4-7535	06 35 30.0	18	9.2	5.6	10.4	-	star	
	-75 35 14		-	1.0	2.5		1	
EXO0651.7+5542	06 51 42.8	30	6.2	5.7	9.5	-	star	
	55 42 05		-	1.3	2.8		3	
EXO0706.1+5913	07 06 7.5	30	5.7	19.5	18.4	41^b	BL-Lac	
	59 13 30		0.125	3.1	0.8	0.5	1	
EXO0708.4+4355	07 08 26.0	30	8.8	8.2	6.9	-	star	HD 54715
	43 55 40		-	1.5	3.0		3	
EXO0718.7+5522	07 18 45.6	30	5.6	155.5	6.5	-	star	HD 57102
	55 22 50		-	10.1	2.6		3	
EXO0718.7+5526	07 18 47.4	30	5.6	5.8	7.7	-	star	HD 237611
	55 26 21		-	1.2	2.9		3	

TABLE 1—*Continued*

Source Name (1)	Right Ascension Declination (1950.0) (2)	Error Radius (arcsec) (3)	N_H (10^{20}) z (4)	Count Rate (counts s^{-1}) (10^{-3}) (5)	m_v α_{ox} (6)	Radio Flux (mJy) α_{ro} (7)	Class Reference (8)	Comment (9)
EXO0719.1+5556	07 19 8.9	30	5.6	3.9	16.0	-	star	
	55 56 58		-	1.0	1.7		1	
EXO0730.8+3156	07 30 49.3	15	5.5	10.5	13.0	$< 6^b$	star	
	31 56 24		-	1.5	2.0		1	
EXO0734.2+3144	07 34 16.0	60	5.1	34.8	7.6	-	star	HD 60800
	31 44 20		-	6.0	2.6		3	
EXO0740.3+5033	07 40 16.3	40	5.6	45.6	5.3	-	star	HD 61931
	50 33 00		-	5.8	2.9		3	
EXO0742.0+7635	07 42 2.0	15	3.8	6.9	12.2	-	star	
	76 35 51		-	0.8	2.2		1	
EXO0748.6+5520	07 48 37.4	15	4.5	23.2	6.4	-	star	HD 63586
	55 20 20		-	2.6	2.9		3	
EXO0753.4+2559	07 53 27.9	30	4.4	3.5	10.3	-	star	
	25 59 08		-	1.0	2.6		3	
EXO0807.5+2758	08 07 32.0	30	3.8	5.7	12.0	-	Class 2	
	27 58 33		-	1.3	2.1			
EXO0811.2+2949	08 11 16.1	30	3.8	5.4	18.3	19^b	BL-Lac	
	29 49 31		-	1.2	1.0	0.4	1	
EXO0811.7+4613	08 11 45.0	30	4.6	3.5	$15.2^\dagger$	$< 6^b$	Gal	MCG8-15-0056
	46 13 37		-	0.8	1.5		3	see text
EXO0848.0+0803	08 48 1.5	20	4.7	23.5	9.9	-	star	IPC
	08 03 05		-	3.0	2.3		3	
EXO0848.0+1228	08 48 4.3	20	3.8	5.2	12.9	$< 6^b$	star	
	12 28 32		-	1.0	2.1		1	
EXO0849.5+0814	08 49 35.5	20	4.7	19.3	6.6	$< 6^b$	star	HD 75767
	08 14 59		-	3.4	2.9		3	IPC
EXO0851.1+2025	08 51 9.0	30	3.0	2.1	8.5	-	star	SAO 80493
	20 25 00		-	0.5	3.0		3	IPC
EXO0855.7+1203	08 55 46.2	30	3.6	5.8	4.3	-	star	HD 76756
	12 03 11		-	1.3	3.4		3	
EXO0905.3-0938	09 05 22.0	15	4.8	3.7	7.8	-	star	HD 78423
	-09 38 43		-	0.6	3.0		3	
EXO0939.3+5608	09 39 19.5	30	1.6	1.8	18.5	-	AGN	
	56 08 32		0.848	0.5	1.2		1	
EXO0940.3+5614	09 40 20.6	30	2.3	3.2	19.3	-	AGN	
	56 14 13		0.197	0.7	1.0		1	
EXO0948.1+1204	09 48 7.9	15	2.8	24.8	6.7	-	star	HD 85259
	12 04 24		-	1.6	2.8		3	
EXO0951.3+6917	09 51 26.0	30	4.5	5.9	11.6	-	AGN	HRI-IPC
	69 17 40		.0008	0.9	$< 2.0^*$		3	M81
EXO0953.7+6918	09 53 47.0	30	4.2	4.3	19.0	-	?	see text
	69 18 06		-	1.1	0.9			HRI-IPC
EXO1000.6+1732	10 00 36.6	15	3.3	2.5	16.0	-	star	
	17 32 53		-	0.5	1.7		1	
EXO1004.0+3509	10 04 0.1	15	2.0	8.8	19.0	6^b	BL-Lac	
	35 09 24		-	1.8	0.9	0.4	1	
EXO1016.8+2007	10 16 51.4	80	2.4	152.5	9.4	-	star	IPC
	20 07 07		-	20.9	2.1		3	AD Leo
EXO1017.0+1943	10 17 1.0	20	2.4	17.2	4.8	-	star	HD 89449
	19 43 35		-	1.3	3.1		3	
EXO1044.0+7155	10 44 3.1	30	3.9	1.7	8.1	-	star	HD 93148
	71 55 03		-	0.5	3.0		3	
EXO1051.0+7005	10 51 3.5	30	2.3	5.0	17.0	$< 6^b$	Gal	
	70 05 31		0.092	1.1	1.3		1	
EXO1055.3+6032	10 55 23.8	20	0.6	14.0	16.7	$< 6^b$	AGN	
	60 32 05		0.149	1.1	1.3		1	
EXO1059.1+7302	10 59 9.2	30	4.2	4.8	16.3	-	AGN	IPC
	73 02 28		0.089	1.0	1.3		7,9	
EXO1059.9+4558	10 59 57.4	30	1.4	3.7	18.3	-	AGN	
	45 58 41		0.764	0.9	1.2		1	
EXO1101.7+4519	11 01 36.0	60	1.0	319.1	18.5	-	C.V.	IPC
	45 19 50		-	34.4	0.6		3	AN UMa
EXO1101.9+3830	11 01 58.2	30	1.8	7.5	7.4	-	star	HD 95976
	38 30 55		-	2.2	2.9		3	HRI

TABLE 1—*Continued*

Source Name (1)	Right Ascension Declination (1950.0) (2)	Error Radius (arcsec) (3)	N_H (10^{20}) z (4)	Count Rate (counts s^{-1}) (10^{-3}) (5)	m_v α_{ox} (6)	Radio Flux (mJy) α_{ro} (7)	Class Reference (8)	Comment (9)
EXO1102.7+2523	11 02 47.6	15	1.7	10.1	18.7	$< 6^b$	AGN	
	25 23 12		0.095	1.2	0.9		8	
EXO1103.0+3829	11 03 3.5	30	1.8	4.6	17.9	-	W.D.	
	38 29 18		-	1.3	1.3		1	
EXO1103.1+2533	11 03 9.0	30	1.5	3.2	17.9		AGN	
	25 33 56		0.625	0.9	1.3		1	
EXO1103.4+2551	11 03 27.4	30	1.5	8.5	17.6	$< 6^b$	AGN	
	25 51 45		0.175	1.8	1.1		1	
EXO1110.4+5520	11 10 24.8	30	0.8	5.0	18.5	-	Class 1	
	55 20 10		-	1.6	1.1			
EXO1113.1+4119	11 13 7.0	35	1.5	13.8	16.4	$< 10^b$	W.D.	see text
	41 19 01		-	2.3	1.4		1	
EXO1113.9+4043	11 13 58.3	30	1.5	7.7	20.8	$< 6^b$	AGN	IPC
	40 43 16		0.200	1.6	0.7		1	
EXO1118.0+4228	11 18 6.1	60	1.9	104.7	17.3	34^b	BL-Lac	
	42 28 10		-	12.9	0.7	0.4	1	
EXO1127.2+4631	11 27 16.0	30	1.7	10.3	8.6	-	star	HD 99900
	46 31 58		-	2.6	2.6		3	
EXO1133.8-3745	11 33 48.4	35	9.1	14.4	10.3	-	star	SAO 202618
	-37 45 30		-	3.2	2.4		3	
EXO1134.5+0156	11 34 32.4	15	2.4	8.5	17.4	-	AGN	
	01 56 27		0.194	1.4	1.1		1	
EXO1138.6+6553	11 38 38.1	30	1.1	3.4	19.1	181^d	AGN	IPC
	65 53 10		0.805	0.8	1.1	0.7	1	
EXO1141.3+2013	11 41 21.8	15	2.2	6.0	18.5	$< 6^b$	AGN	HRI-IPC
	20 13 30		0.335	1.1	1.0		3	
EXO1145.1+0031	11 45 7.1	30	2.4	8.9	19.2	$< 3^a$	AGN	IPC
	00 31 42		0.096	2.0	0.8		1	
EXO1146.9+2455	11 46 54.6	40	2.1	32.4	18.0	13^b	BL-Lac	IPC
	24 55 36		-	2.9	0.8	0.4	1	
EXO1155.5+3233	11 55 32.8	15	1.8	3.2	6.4	$< 6^b$	star	HD 103928
	32 33 05		-	0.6	3.2		3	
EXO1155.8+8057	11 55 53.5	15	4.7	7.9	11.7	-	star	
	80 57 08		-	1.3	2.2		1	
EXO1156.2+3240	11 56 16.5	15	1.9	3.4	16.0	-	star	
	32 40 11		-	0.6	1.7		1	
EXO1156.3+3239	11 56 19.7	30	1.7	2.7	18.5	-	AGN	
	32 39 05		0.215	0.6	1.1		1	
EXO1156.5+3239	11 56 30.8	30	1.7	2.4	16.5	-	star	
	32 39 51		-	0.6	1.7		1	
EXO1158.6-0323	11 58 40.8	30	3.5	11.3	15.3	$< 6^a$	AGN	IPC
	-03 23 55		0.019	2.7	1.3		1	
EXO1201.3+4508	12 01 18.6	15	1.3	5.3	8.9	-	star	HD 104753
	45 08 14		-	0.6	2.7		3	IPC
EXO1201.6+4448	12 01 38.2	18	1.3	3.0	15.5	$< 6^b$	Class 1	IPC
	44 48 20		-	0.4	1.6			Galaxy (POSS)
EXO1204.9+4731	12 04 58.0	30	2.0	5.8	11.1	-	star	
	47 31 20		-	1.5	2.4		1	
EXO1205.8+5256	12 05 52.3	30	1.5	4.1	17.3	-	AGN	
	52 56 49		0.435	0.9	1.3		1	
EXO1207.9+3945	12 07 55.2	30	2.1	5.5	19.1	6^c	BL-Lac	HRI-IPC
	39 45 44		0.615	1.7	0.9	0.4	9	
EXO1215.3+3022	12 15 18.7	70	1.6	58.8	15.6	420^c	BL-Lac	IPC
	30 22 20		-	6.7	1.1	0.5	3	ON 325
EXO1215.9+3004	12 15 59.0	55	1.7	114.7	14.0	-	AGN	IPC
	30 04 40		0.012	8.3	1.2		3	MKN 766
EXO1216.6+7526	12 16 36.0	30	3.4	13.3	5.4	-	star	HD 107193
	75 26 20		-	3.7	3.1		3	
EXO1218.8+3027	12 18 50.9	30	1.7	190.1	16.5	52^c	BL-Lac	HRI
	30 27 06		-	14.1	0.8	0.4	3	3A 1218+303
EXO1219.2+0213	12 19 14.5	25	1.9	6.3	12.8	-	star	
	02 13 25		-	1.2	2.1		1	
EXO1219.5+3019	12 19 30.5	30	1.7	6.1	14.5	-	Gal	RNGC 4380
	30 19 08		-	1.9	1.6		3	

TABLE 1—*Continued*

Source Name (1)	Right Ascension Declination (1950.0) (2)	Error Radius (arcsec) (3)	N_H (10^{20}) z (4)	Count Rate (counts s^{-1}) (10^{-3}) (5)	m_v α_{ox} (6)	Radio Flux (mJy) α_{ro} (7)	Class Reference (8)	Comment (9)
EXO1222.5+1640	12 22 32.5	30	2.5	3.5	19.4	< 7	AGN	IPC
	16 40 36		0.184	1.0	0.9		1	
EXO1226.6+4200	12 26 37.1	18	1.8	17.1	12.9	-	star	
	42 00 23		-	1.8	1.9		3	
EXO1228.7+1219	12 28 42.2	30	2.4	4.0	17.1	-	AGN	
	12 19 40		0.116	1.2	1.2		3	
EXO1233.3-3935	12 33 18.6	15	5.9	31.8	5.8	-	star	HD 109573
	-39 35 46		-	1.8	2.9		3	IPC
EXO1249.7-2858	12 49 43.4	40	6.1	274.9	13.0	-	C.V.	HRI-IPC
	-28 58 27		-	17.4	1.4		3	EX Hya
EXO1251.7+2611	12 51 43.3	35	1.0	16.6	18.4	-	AGN	
	26 11 54		0.196	3.1	1.0		1	
EXO1259.0+2807	12 59 3.0	35	0.9	16.7	18.4	< 6[b]	AGN	IPC
	28 07 10		0.243	2.7	1.0		10	
EXO1259.6+1238	12 59 36.3	30	2.3	11.7	11.5	-	star	
	12 38 28		-	2.8	2.2		11	
EXO1259.6+2803	12 59 37.9	25	0.9	7.5	17.1	-	Gal	IPC
	28 03 04		0.023	0.9	1.3		10	
EXO1300.3+2809	13 00 22.5	30	0.9	1.3	20.1	-	AGN	
	28 09 44		0.510	0.3	1.1		1	
EXO1307.3-0516	13 07 21.7	45	2.6	67.4	4.4	-	star	
	-05 16 30		-	4.7	2.0		3	
EXO1309.1+3207	13 09 08.5	30	1.1	13.5	16.2	< 10[b]	Gal	IPC
	32 07 42		0.072	2.8	1.3		1	
EXO1309.7+3229	13 09 44.0	30	1.1	6.2	14.1	-	star	IPC
	32 29 18		-	1.7	1.9		1	
EXO1321.8-0203	13 21 49.5	25	2.2	22.9	8.8	-	star	HD 116554
	-02 03 06		-	3.4	2.6		3	
EXO1326.1+7944	13 26 12.0	30	4.0	3.6	17.8	-	AGN	
	79 44 23		0.143	0.9	1.1		1	
EXO1331.7-3120	13 31 46.0	30	3.9	4.9	14.5	< 12[a]	Class 2	IPC
	-31 20 28		-	1.0	1.6			
EXO1335.8-2918	13 35 53.2	15	4.0	4.1	5.8	-	star	HD 118646
	-29 18 28		-	0.8	3.2		3	IPC
EXO1342.8-3247	13 42 49.2	25	4.0	37.5	4.2	-	star	HD 119756
	-32 47 37		-	3.8	3.1		3	
EXO1346.2+2637	13 46 15.8	15	1.5	8.8	19.1	< 6[b]	AGN	HRI-IPC
	26 37 21		0.915	0.9	0.9		1	
EXO1346.2+2645	13 46 16.7	30	1.1	2.5	17.5	-	AGN	IPC
	26 45 51		0.059	0.7	1.4		1	
EXO1346.4+2637	13 46 29.6	15	1.5	3.9	18.1	-	AGN	
	26 37 30		0.597	0.6	1.2		1	
EXO1346.7+2713	13 46 45.0	40	1.1	17.7	7.0	-	star	HD 120476
	27 13 16		-	2.1	2.8		3	
EXO1352.2+1838	13 52 17.5	30	2.0	23.6	2.7	-	star	HD 121370
	18 38 30		-	3.4	3.4		3	IPC
EXO1415.2+2607	14 15 12.6	15	2.3	4.2	18.8	< 6[a]	AGN	
	26 07 27		0.184	0.6	1.0		1	
EXO1415.6+2557	14 15 40.6	15	1.6	50.1	16.0	54[c]	BL-Lac	IPC
	25 57 45		0.237	5.8	1.1	0.4	12	
EXO1416.3-1308	14 16 23.1	30	6.4	4.4	4.5	-	star	HD 125337
	-13 08 19		-	0.9	3.4		3	
EXO1429.9+3717	14 29 58.5	65	1.0	35.1	21.0	-	AGN	
	37 17 05		1.925	5.7	0.4		1	
EXO1431.6+3637	14 31 38.3	30	1.0	1.8	14.2	-	star	
	36 37 50		-	0.5	2.0		1	
EXO1459.9-3227	14 59 55.3	40	9.7	398.6	5.4	-	star	HD 132955
	-32 27 11		-	24.4	2.6		3	
EXO1502.0+4749	15 02 5.0	65	2.2	295.9	4.8	-	star	HD 133640
	47 49 50		-	34.3	2.7		3	IPC
EXO1550.5+1905	15 50 34.1	40	3.8	57.6	14.9	-	C.V.	PG1550+191
	19 05 05		-	6.3	1.4		3	MR Ser
EXO1553.4+1845	15 53 24.4	30	3.2	65.9	6.3	-	star	HD 142763
	18 45 55		-	5.9	2.7		3	

TABLE 1—*Continued*

Source Name (1)	Right Ascension Declination (1950.0) (2)	Error Radius (arcsec) (3)	N_H (10^{20}) z (4)	Count Rate (counts s^{-1}) (10^{-3}) (5)	m_v α_{ox} (6)	Radio Flux (mJy) α_{ro} (7)	Class Reference (8)	Comment (9)
EXO1556.4+2659	15 56 25.5	30	4.6	5.2	8.7	-	star	HD 143271
	26 59 49		-	1.1	2.8		3	
EXO1600.1+1610	16 00 6.7	30	3.3	12.8	15.0	-	Class 1	
	16 10 26		-	2.5	1.4			
EXO1612.0+3353	16 12 3.4	30	1.7	3.5	12.9	-	star	
	33 53 53		-	0.8	2.2		1	
EXO1615.6+0624	16 15 37.5	30	4.6	4.3	13.3	$< 6^b$	star	
	06 24 13		-	1.0	2.1		1	
EXO1622.0+2611	16 22 3.2	40	3.7	10.3	16.8	-	AGN	
	26 11 12		0.040	2.0	1.1		1	
EXO1627.3+4014	16 27 21.0	40	0.9	54.2	19.0	22^b	AGN	see text
	40 14 04		0.27	6.5	.7	0.5	1	
EXO1652.4+3930	16 52 27.2	15	1.6	14.6	17.5	$< 15^b$	AGN	IPC
	39 30 20		0.070	2.9	1.1		1	
EXO1652.8-0818	16 52 52.6	15	13.1	9.5	16.9	-	star	VB 8
	-08 18 38		-	1.1	1.4		13	HRI
EXO1659.7+3338	16 59 45.6	15	1.9	21.7	5.3	-	star	HD 154029
	33 38 25		-	3.5	3.1		3	
EXO1709.6+3339	17 09 41.0	30	2.5	4.6	17.2	$< 6^b$	AGN	
	33 39 12		0.471	1.1	1.2		1	
EXO1807.7+7845	18 07 45.0	15	3.9	2.0	11.5	-	star	IPC
	78 45 31		-	0.4	2.5		7	see text
EXO1808.3-6456	18 08 22.1	30	6.5	2.8	12.5	-	star	see text
	-64 56 06		-	0.7	2.3		3	
EXO1809.4+7822	18 09 24.8	25	3.9	8.5	17.8	$< 6^b$	star	
	78 22 20		-	1.5	1.3		1	
EXO1810.3+6940	18 10 22.1	20	5.4	13.3	9.0	-	star	HD 167605
	69 40 09		-	1.2	2.6		3	IPC
EXO1811.5+4128	18 11 31.0	30	3.6	4.7	7.4	31^d	star	HD 167389
	41 28 08		-	1.3	3.0	-0.3	3	
EXO1811.7+3143	18 11 43.1	30	5.5	3.2	17.4	105^b	BL-Lac	
	31 43 18		0.117	0.7	1.2	0.5	1	
EXO1814.0+4208	18 14 5.7	45	3.6	244.3	5.5	-	star	HD 167965
	42 08 25		-	16.4	2.6		3	
EXO1815.1+5013	18 15 10.0	30	4.3	2.7	8.9	-	star	HD 234601
	50 13 05		-	0.8	2.9		3	
EXO1819.2+5038	18 19 15.4	30	4.5	1.1	14.4	-	star	
	50 38 40		-	0.3	2.2		1	
EXO1821.6+6420	18 21 36.0	15	3.5	26.4	15.0†	-	Pl. Neb.	IPC
	64 20 09		-	2.3	1.7		3	DS Dra
EXO1821.6+6419	18 21 40.6	15	3.5	51.7	14.1	-	AGN	IPC
	64 19 00		0.297	2.2	1.3		3	
EXO1824.9+6447	18 24 59.9	55	4.1	22.1	7.1	-	star	HD 170527
	64 47 40		-	3.2	2.8		3	IPC
EXO1827.8-6518	18 27 55.7	45	6.5	15.8	7.9	-	star	HD 170196
	-65 18 02		-	2.0	2.7		3	
EXO1831.0+5204	18 31 4.1	30	4.0	26.0	6.6	-	star	HD 171461
	52 04 24		-	2.4	2.9		3	
EXO1833.1+5104	18 33 10.9	65	4.5	39.0	7.8	-	star	HD 171871
	51 04 36		-	6.2	2.6		3	
EXO1839.6+8002	18 39 36.8	15	4.1	17.2	13.2	-	star	IPC
	80 02 47		-	2.0	1.9		11	
EXO1859.2+6927	18 59 15.1	40	7.0	57.0	6.3	-	star	HD 177410
	69 27 50		-	4.9	2.8		3	
EXO1905.1+7001	19 05 6.1	30	7.0	3.8	11.6	-	star	
	70 01 40		-	0.9	2.4		1	
EXO1928.7+7403	19 28 47.3	30	7.8	2.9	10.5	-	star	
	74 03 12		-	0.7	2.7		1	
EXO1948.4-4000	19 48 26.0	15	7.4	34.4	5.3	-	star	HD 187474
	-40 00 10		-	4.9	3.0		3	
EXO2000.3-5611	20 00 18.2	15	5.8	68.3	15.2	$< 9^a$	W.D.	
	-56 11 04		-	4.5	1.3		1	
EXO2005.4+7238	20 05 28.9	30	10.7	3.9	7.7	-	star	HD 191634
	72 38 13		-	0.9	3.0		3	

TABLE 1—*Continued*

Source Name (1)	Right Ascension Declination (1950.0) (2)	Error Radius (arcsec) (3)	N_H (10^{20}) z (4)	Count Rate (counts s^{-1}) (10^{-3}) (5)	m_v α_{ox} (6)	Radio Flux (mJy) α_{ro} (7)	Class Reference (8)	Comment (9)
EXO2014.8-5731	20 14 53.0	15	5.8	64.1	13.0	-	W.D.	
	-57 31 10		-	3.1	1.7		3	
EXO2128.7+1154	21 28 44.3	18	6.7	56.3	6.0	-	star	HD 204862
	11 54 59		-	2.4	2.8		3	
EXO2157.0-3146	21 57 2.0	30	1.7	24.3	7.0	-	star	HD 208886
	-31 46 16		-	2.8	2.8		3	
EXO2159.6-3222	21 59 38.6	35	1.7	31.8	6.6	-	star	HD 209253
	-32 22 14		-	3.5	2.8		3	
EXO2205.1-4712	22 05 6.9	15	1.8	6815.2	1.7	-	star	HD 209952
	-47 12 30		-	211.7	2.6		3	
EXO2205.7-4725	22 05 44.0	15	2.3	13.4	12.5	5[a]	star	
	-47 25 21		-	2.2	2.0		1	
EXO2214.6-0902	22 14 41.0	50	5.1	37.4	13.5	-	star	
	-09 02 40		-	4.4	1.7		1	
EXO2217.5-0804	22 17 31.5	60	5.2	124.0	5.4	-	star	HD 211838
	-08 04 10		-	14.2	2.7		3	
EXO2221.5-0505	22 21 30.6	35	5.7	67.3	5.8	-	star	HD 212404
	-05 05 40		-	6.3	2.8		3	IPC
EXO2232.4-3733	22 32 29.7	15	1.2	5.0	17.7	< 6[a]	AGN	
	-37 33 48		0.209	0.8	1.2		1	
EXO2251.1-1737	22 51 10.4	30	2.8	2.2	16.0	-	star	IPC
	-17 37 55		-	0.5	1.8		1	
EXO2306.0+0425	23 06 1.3	30	5.1	6.6	8.1	-	star	HD 218515
	04 25 00		-	1.7	2.8		3	
EXO2317.8+1630	23 17 52.7	30	4.6	3.8	10.4	-	star	
	16 30 59		-	0.8	2.6		3	
EXO2317.9+1652	23 17 56.2	30	4.0	2.1	19.0	-	AGN	
	16 52 53		0.300	0.5	1.0		1	
EXO2318.4+1658	23 18 27.3	30	4.6	3.2	6.7	-	star	HD 220091
	16 58 43		-	0.7	3.2		3	
EXO2318.5-2715	23 18 34.5	40	2.1	174.7	5.6	-	star	HD 220096
	-27 15 39		-	12.5	2.6		3	
EXO2340.8-1512	23 40 53.0	15	1.7	84.6	15.7	8[a]	AGN	IPC
	-15 12 20		0.137	6.2	1.0	0.2	1	
EXO2352.5+0648	23 52 33.3	60	5.7	45.2	6.2	-	star	HD 224103
	06 48 15		-	7.3	2.8		3	

REFERENCES.—(1) This paper; (2) Tagliaferri et al. 1988; (3) SIMBAD data bank; (4) IAU Circ., No. 4172; (5) Beuermann et al. 1989; (6) Osborne et al. 1988; (7) Gioia et al. 1990; (8) Beuermann, Stella, & Sieber 1984; (9) Stocke et al. 1991; (10) Branduardi-Raymont et al. 1985; (11) Caillault et al. 1986; (12) Halpern et al. 1986; (13) Tagliaferri, Doyle, & Giommi 1990.

[a] 8.4 GHZ, this paper.

[b] 5 GHz, this paper.

[c] 5 GHz, Véron-Cetty, & Véron 1989.

[d] 5 GHz, Becker et al. 1991.

* An upper limit is given, since m_v refers to the whole galaxy and not to the nucleus where most of the X-ray emission originates.

† m_b.

have been detected just above the detection threshold; column (4) gives the Galactic hydrogen column density N_H along the line of sight estimated from 21 cm radio measurements (Stark et al. 1984 and Parkes data) and redshift (if appropriate) of the optical counterpart; column (5) gives the count rate with error (including both statistical and systematic uncertainties) on the following line; column (6) gives the visual apparent magnitude[14] of the optical counterpart (or of the brightest object in the error box if the source is not identified) and its optical to X-ray spectral slope (α_{ox}); column (7) gives the radio flux at 5 or 8.4 GHz when available, and the radio to optical spectral slope (α_{ro}); column (8) gives the source class according to the following code: AGN = emission-line active galactic nuclei, CV = cataclysmic variable, BL-Lac = BL Lacertae object, star = star, W.D. = white dwarf, Gal = "normal galaxy," Pl. Neb = planetary nebula; finally, column (9) contains comments. If a source is unidentified (see next paragraph), classification is tentatively assigned on the basis of its X-ray to optical flux ratio (e.g., Maccacaro et al. 1988). The source is classified as class 1 (i.e., likely to be extragalactic) if its log (f_x/f_{opt}) [defined as $\log (f_x/f_{opt}) = \log f_x + m_V/2.5 + 5.37$, where f_x is the 0.3–3.5 keV flux in ergs cm^{-2} s^{-1} assuming $\alpha = 1.5$] is greater than 0.0 or if the object is extended (galaxy) on the Palomar plate, and as class 2 otherwise.

The conversion between the count rate, given in Table 1, and flux can vary strongly from source to source. A proper conversion can be obtained using the plots shown in Figures 2a and 2b.

A cross-correlation with the *Einstein* IPC and high-resolution imager (HRI) source lists shows that 63 sources

[14] Whenever possible, the magnitudes were measured directly from the optical spectra or taken from the literature; in all other cases magnitudes were estimated from POSS or ESO plates. Magnitude errors are expected to be of the order of 1.0 mag or less.

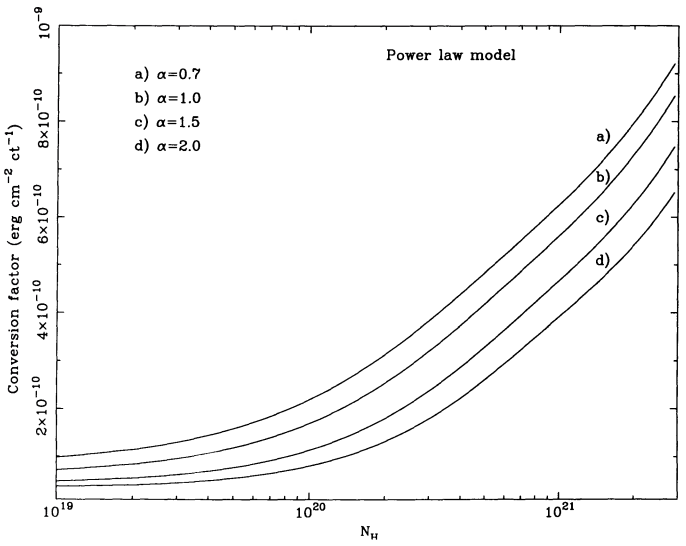

FIG. 2a

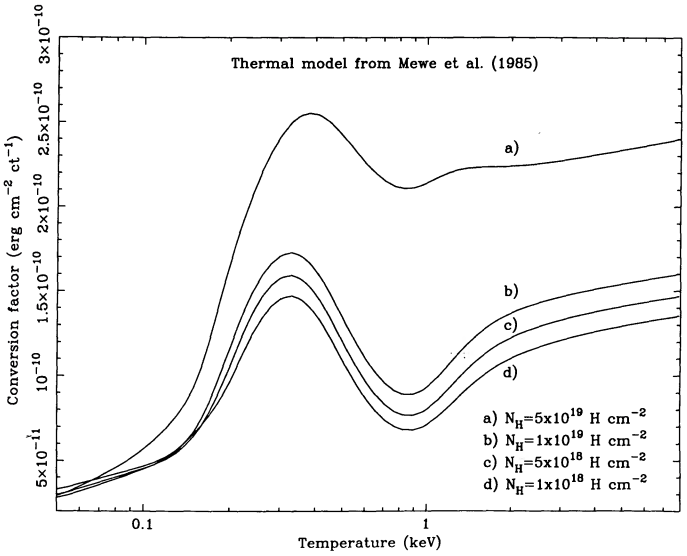

FIG. 2b

FIG. 2.—(*a*) Plot of the conversion factor between a count rate of 1.0 counts s^{-1} and flux in units of ergs cm^{-2} s^{-1} in the 0.05–2.0 keV energy band for various values of the spectral index, α = (0.7, 1.0, 1.5, and 2.0) as a function of Galactic N_H. (*b*) Same as (*a*) but for the thermal model of Mewe, Gronenschild, & Van den Oord (1985) that is appropriate for coronal emission sources.

were also detected by the IPC and 12 by the HRI (see Tables 1 and 2). Two of the still unidentified objects are IPC sources.

6. THE IDENTIFICATION PROGRAM

The process of identification of the serendipitous X-ray sources in the HGLS was performed in two steps:

1. Cross-correlation between the list in Table 1 and several catalogs of known objects available in computer-readable format, including catalogs of QSO and Seyfert galaxies (e.g., Hewitt & Burbidge 1987; Véron-Cetty & Véron 1989), the Bright Star Catalogue (Hoffleit & Jaschek 1982) the HD star catalog, and the data bank of the Strasbourg Astronomical Data Center, SIMBAD.
2. An extensive program of optical and radio observations carried out over the past three years.

A source in one in the catalogs was accepted as the counterpart of the X-ray source if (*a*) its position is within (or very close to) the X-ray error circle, (*b*) its X-ray to optical flux ratio is typical of the class of sources to which the object belongs (e.g., Stocke et al. 1983; Gioia et al. 1984), and (*c*) no other plausible candidates with magnitude brighter than the Palomar Sky Survey limit (or ESO plates for southern objects) are present in the X-ray error circle. When this process did not produce a reliable identification, optical and radio observations were carried out of the sources inside or immediately outside the X-ray error circle. In about 50% of the cases all candidate counterparts were observed at optical frequencies; however, because of the limited observing time, in all the remaining cases observations were stopped when a plausible counterpart was found. Because of the relatively small error circles, and since all sources are well above the Galactic plane, we do not expect this procedure to have produced more than 2–3 misidentifications.

The optical observations were performed with the 2.2 m ESO/MPI telescope in La Silla, the 2.2 m and 3.6 m MPI telescopes at Calar Alto, the 4.2 m William Herschel Telescope (WHT) and the 2.5 m Isaac Newton Telescope (INT) on La Palma, and the 3.9 m Anglo-Australian Telescope. The radio observations were performed with the (5 km) Cambridge and the Parkes radio telescopes. Details of these observations will be published elsewhere.

This procedure has so far produced an optical identification for 200 of the 210 sources in the sample. Since the remaining 10 objects have been preliminarily identified on the basis of their X-ray to optical flux ratio, which is a fairly accurate predictor (Gioia et al. 1984), the sample can be considered as essentially fully identified.

The distribution of the positions of the optical counterparts with respect to the X-ray positions is consistent with the error radii given in Table 1.

7. ADDITIONAL X-RAY SOURCES

In addition to the objects included in Table 1, 23 other serendipitous sources that did not satisfy all the criteria for inclusion in the complete sample were identified during the optical/radio campaign. These sources are listed in Table 2. Of the 23 sources included in this table, 12 are AGNs, two are BL Lacs, seven are stars, one is a white dwarf, and one is an AM Herculis–type object.

8. OPTICAL DATA

Eight identification runs were carried out between 1986 and 1989 with the 2.2 m telescope at La Silla during MPI time and the 3.5 m telescope of the Deutsch-Spanisch Astronomisches Zentrum at Calar Alto, Spain. Comparatively low-resolution spectroscopy was performed at both telescopes using Boller & Chivens spectrographs equipped with RCA CCDs. Spectral coverage was 4100–7500 Å at La Silla and 3800–7200 Å at Calar Alto, with resolutions of about 10 Å FWHM. Some La Silla spectra cover a range of 3400–10000 Å with 20 Å FWHM resolution.

Optical spectroscopy was also carried out during a total of 3

TABLE 2

ADDITIONAL CMA SERENDIPITOUS SOURCES

Source name	Right Ascen. Declination (1950.0)	erorr radius (arcsec)	N_H (10^{20}) z	count rate $cts\ s^{-1}$ (10^{-3})	m_v α_{ox}	Radio flux (mJy) α_{ro}	class ref.	comment
(1)	(2)	(3)	(4)	(5)	(6)	(7)	(8)	(9)
EXO0012.6-7307	00 12 40.2	15	2.8	40.3	12.7	-	star	IPC
	-73 07 13		-	1.8	1.8	-		
EXO0017.3-2538	00 17 21.6	15	2.5	13.1	16.6	-	AGN	
	-25 38 45		0.129	1.9	1.1			
EXO0059.8-2218	00 59 48.1	15	1.5	6.9	18.1	< 7[a]	AGN	IPC
	-22 18 14		0.235	0.9	1.1			
EXO0122.0+0835	01 22 5.6	30	4.3	1.4	18.0	-	AGN	
	08 35 52		0.166	0.5	1.2			
EXO0234.5-5232	02 34 31.3	15	2.0	8.7	18.7	-	CV	AM Her type
	-52 32 18		-	1.4	1.1			
EXO0235.3-5236	02 35 21.5	15	2.0	6.8	17.2	< 5[a]	AGN	HRI
	-52 36 36		0.113	1.1	1.2			
EXO0330.6-2613	03 30 41.0	30	1.0	7.6	19.1	< 8[a]	AGN	IPC
	-26 13 07		0.663	1.9	1.0			
EXO0408.4-7134	04 08 28.8	15	3.3	5.1	12.5	-	star	
	-71 34 47		-	0.9	2.1			
EXO0414.4+1206	04 14 29.5	25	15.5	12.4	15.2	-	star	
	12 06 42		-	3.2	1.7			
EXO0423.4-0840	04 23 26.2	30	6.2	3.1	15.9	34[a],45[b]	BL-Lac?	MCG01-12-005
	-08 40 28		0.039	1.1	1.4	0.3		See text
EXO0507.1-0404	05 07 9.9	15	7.5	17.2	19.0	27[a]	BL-Lac	
	-04 04 20		0.304	4.0	0.6	0.5		
EXO0734.0+1723	07 34 6.0	25	4.7	6.1	17.3	< 4[a]	AGN	IPC
	17 23 14		0.199	1.2	1.1			
EXO0812.5+2955	08 12 30.3	30	3.8	12.6	12.3	-	star	
	29 55 50		-	2.7	2.1			
EXO0917.3-0722	09 17 22.7	15	3.7	10.5	17.1	< 5[a]	AGN	
	-07 22 58		0.169	1.3	1.1			
EXO0947.3+8545	09 47 20.0	65	6.9	85.0	16.5	-	W.D.	
	85 45 23		-	11.7	1.1			
EXO1102.7+2523	11 02 47.6	15	1.7	10.1	18.7	-	AGN	
	25 23 10		0.095	1.2	0.9			
EXO1128.1+6908	11 28 8.0	25	1.3	43.2	16.5	-	AGN	
	69 08 42		0.044	5.6	1.1			
EXO1229.9+2039	12 29 55.1	15	2.8	9.1	13.7	-	star	IPC
	20 39 49		-	2.3	2.0			
EXO1839.1-7835	18 39 8.6	15	5.0	8.6	15.6	< 65[a]	AGN	
	-78 35 02		0.074	1.2	1.3			
EXO1946.7-4007	19 46 44.9	18	4.7	9.6	15.9	131[a]	AGN	
	-40 07 50		0.106	3.2	1.3	0.4		
EXO2032.9-3617	20 32 55.3	25	3.5	44.0	11.7	-	star	+ Gal m_v = 16.8
	-36 17 34		-	4.0	1.7			see text
EXO2041.8-3129	20 41 51.7	15	5.0	26.8	14.6	< 7[a]	star	
	-31 29 11		-	8.5	1.6			
EXO2231.7-3758	22 31 46.0	30	1.2	12.4	16.6	< 7[a]	AGN	
	-37 58 18		0.141	2.1	1.3			

[a] 8.4 GHz.
[b] 5 GHz.

weeks of observing time with the William Herschel Telescope and the faint object spectrograph on La Palma in 1988 February and June. The wavelength range covered by the spectra was 3500–10000 Å with 13 Å FWHM spectral resolution. During this campaign, 30 sources were identified. Two sources were identified using the Isaac Newton Telescope and the image photon counting system (IPCS) during observing runs at La Palma in 1986 and 1987. The spectra covered the wavelength range 3500–7500 Å with a resolution of 6 Å FWHM. Finally, four objects were identified in the course of a three-night observing run with the Anglo-Australian Telescope in 1989 January, when the combination of the faint object red spectrograph (FORS) and the IPCS was used. The FORS provided a resolution of 10 Å FWHM over the range 5500–9500 Å; the IPCS was used in the blue (3500–5500 Å), with a resolution of 1.5 Å FWHM.

The optical characteristics of the AGNs we have identified are very similar to those of other X-ray and optically selected AGNs. Preliminary results of some of the optical data are presented in Branduardi-Raymont et al. (1989). Final results, together with finding charts and all the details of the optical observations, will be published in Thomas et al (1991) and Mittaz et al. (1991). Copies of the finding charts can be obtained before publication from P. Giommi.

9. RADIO DATA

Radio observations of 57 sources were performed using the 5 km Cambridge and the Parkes radio telescopes. Observations

at the Parkes 64 m radio telescope were performed on 1988 April 7. An 8.4 GHz cooled FET receiver with a system noise temperature of less than 60 K was used, together with a switching dual-beam feed which permitted observations of the target and background regions on either side. The separation of the two beams was 6'.7, and their half-power beamwidth was 2'.7. The observations were conducted in two orthogonal switching directions, so that four surrounding background regions were sampled during the pair of exposures, each of 11 minute duration.

The observations with the Cambridge 5 km telescope were made over a period from 1986 to 1989, and each consisted of one 12 hr observation; as a result of engineering work, some of the antennas were from time to time out of commision, worsening the sensitivity slightly. For most of the observations the rms noise level was 1–1.5 mJy. The frequency was 4.995 GHz with a 10 MHz bandwidth. In those cases for which nondetection was achieved, a reasonable conservative upper limit of 6 mJy is suggested.

Fifteen sources out of 57 were detected at 5 or 8.4 GHz. This detection rate, however, is not statistically meaningful, since the targets of the radio observations were not chosen in a random way.

In addition to direct radio measurements, a cross-correlation between all objects in our sample and a catalog containing 53,522 northern radio sources (Becker, White, & Edwards 1991) has been performed. The catalog is characterized by limiting sensitivity in the range 20–40 mJy and was constructed using 4.85 GHz observations performed with the 300 foot (91 m) NRAO Green Bank telescope (Condon, Broderick, & Seielstad 1989). Eight sources in our sample have been found to lie within the combined radio/X-ray error regions. Six of these were also detected during our observations, and the intensities reported in Table 1 are from our measurements.

10. COMMENTS ON INDIVIDUAL SOURCES

10.1. *EXO 0044.4+2001*

This X-ray source has an 18 mag optical counterpart and a radio flux density of 61 mJy at 8 GHz. These intensities place EXO 0044.4+2001 in the area of the α_{ox}-α_{ro} diagram populated by BL Lac objects and radio-emitting AGNs (see, e.g., Fig. 6*b* of Stocke et al. 1991).

10.2. *EXO 0234.5−5232, EXO 0329.9−2606, EXO 0333.3−2554*

These serendipitous sources are optically faint and previously unknown AM Herculis–type objects. AM Herculis systems are very rare, and only about 15 such systems are presently known (e.g., Beuermann 1988). Although the *EXOSAT* HGLS covered a very small fraction of the sky ($\approx$3%), it includes four such systems (the three listed above plus PG 1550+191), thus proving that soft X-ray surveys are probably the most effective way of discovering new sources of this kind. Detailed description of the X-ray and optical data for EXO 0234.5−5232, EXO 0329.9−2606, and EXO 0333.3−2554 can be found in Osborne et al. (1988), Beuermann et al. (1987, 1990), and Beuermann, Thomas, & Schwope (1988).

10.3. *EXO 0423.4−0840*

This source is identified with the galaxy MCG 01-12-005, which is a radio source and shows no emission lines. This object is located in the region of the α_{ox}-α_{ro} diagram that is populated by AGNs and BL Lac objects. Since no strong emission lines have been detected from MCG 01-12-005 and its X-ray luminosity is in excess of 10^{43} ergs s^{-1}, we consider EXO 0423.4−0840 to be a candidate BL Lac object.

10.4. *EXO 0811.7+4613*

This spiral galaxy is included in the *IRAS* Point Source Catalog and has been proposed as a candidate AGN (De Grijp, Miley, & Lub 1987) on the basis of its *IRAS* colors. However, since no optical spectrum is available, we prefer to be conservative and preliminarily classify this object as a galaxy.

10.5. *EXO 0953.7+6918*

This source was detected 3 times by *EXOSAT*, and during *Einstein* IPC and HRI pointed observations. EXO 0953.7+6918 is also included in the IPC slew survey (Elvis, Plummer, & Fabbiano 1990) list. The *EXOSAT* and *Einstein* positions agree very well, and the X-ray flux remained constant during all the observations. There are three very faint objects ($m_v > 19.0$) inside or near the error circle ($\approx 10''$), and all are stars. Since the X-ray to optical flux ratio is unacceptably high for nonflaring stars, we conclude that there is no plausible optical counterpart to EXO 0953+6918 that is brighter than the Palomar plates limit.

10.6. *EXO 1113.1+4119*

The error circle includes a 16.4 mag white dwarf and a much fainter ($m_v = 19.9$) emission-line object at redsift $z = 0.16$.

10.7. *EXO 1627.3+4014*

The probable counterpart given in Table 1 is a 19 mag AGN with broad emission lines at $z = 0.27$ which was also detected as a radio source. A CCD image shows several other faint objects in or near the X-ray error box, two of which are narrow emission-line objects with $z = 0.27$. Hence, this may be a distant cluster of galaxies.

10.8. *EXO 1807.7+7845*

This source is included in the *Einstein* EMSS, where it has been classified as a star (Gioia et al. 1990). However, EXO 1897.7+7845 (=MS 1807.8+7846) has also been identified with a steep spectrum radio source possibly associated with a very faint cluster of galaxies (Johnston et al. 1984). EXO 1807+7845 has been detected in the CMA as a pointlike source on three different occasions. The *EXOSAT* position, which has an associated 90% error circle of 15″, is centered on the star, strongly suggesting that the stellar candidate is the counterpart of the X-ray detection, thus confirming the EMSS classification.

10.9. *EXO 1808.3−6456*

The error box of this source includes a 12th magnitude O subdwarf and a second fainter and still unidentified object.

10.10. *EXO 2032.9−3617*

The error circle of EXO 2032.9−3617 includes two candidate counterparts: a 11.7 mag dm(e) star and a 16.8 mag galaxy ($z = 0.087$ in absorption). If the star is assumed to be the counterpart of the EXO 2032.9−3617, its X-ray to optical flux ratio is typical of this class of objects. If the galaxy is assumed to be the counterpart, its X-ray to optical flux ratio is too high

for a normal galaxy and its X-ray luminosity is in the range 3×10^{44} to 1×10^{45}. However, the galaxy shows no emission lines and could be a BL Lac object, in which case both the flux ratio and the high X-ray luminosity would be explained. Since we have no radio measurements of this area, we cannot decide which of the two objects is the most likely counterpart of the X-ray source.

11. STATISTICAL PROPERTIES

The complete sample includes most classes of known X-ray emitters. Table 3 lists the number of detected objects for each class.

A plot of the logarithm of the X-ray to optical flux ratio, log (f_x/f_{opt}), versus apparent optical magnitude, m_v, is shown in Figure 3. In this graph early-type stars are shown as open stars, late-type stars as filled stars, BL Lacs as open circles, emission-line AGNs as filled circles, white dwarfs as squares, cataclysmic variables as plus signs, galaxies as crosses, and unidentified objects as triangles. A fairly clear separation between different classes of X-ray sources similar to that of the EMSS (Stocke et al. 1983; Gioia et al. 1984) is apparent. A small fraction of late-type stars, however, falls in the region normally occupied by galaxies and AGNs. The flux of all AGNs was calculated assuming a power-law model with energy index 1.5 and N_H equal to the Galactic value; a constant conversion between count rate and flux equal to 1×10^{-10} ergs cm^{-2} count^{-1} (Pallavicini et al. 1988; see also Fig. 2*b*) was instead used for stellar sources. The count rate of several *early-type* (black stars in Fig. 3) probably includes a substantial contribution from UV radiation due to a small transparency of the thin Lexan filter to UV photons (e.g., Chiappetti & Giommi 1985). Since the amount of UV radiation is impossible to estimate without knowing precisely the optical characteristics of each star, no correction to remove this contribution has been attempted here.

The distributions of m_v of all the sources in the complete sample is shown in Figure 4 (*dotted histogram*), where two peaks, roughly corresponding to Galactic and extragalactic sources, are clearly visible. The solid histogram represents extragalactic sources only and is strongly peaked at around $m_v \approx 17$–18. The average apparent magnitude $\langle m_v \rangle$ is 17.4, a value similar to that of the EMSS (e.g., Gioia et al. 1986). The redshift distribution of AGNs (Fig. 5) peaks at very low values of z, and the average value $\langle z \rangle = 0.33$ is slightly lower than that of the EMSS ($\langle z \rangle = 0.4$; Gioia et al. 1986). This difference is not surprising, since the sensitivity limit of the HGLS is on average approximately a factor of 5 worse than that of the EMSS.

TABLE 3

OPTICAL IDENTIFICATIONS

Source Type	Number of Sources
Early-type stars	50
Late-type stars	77
Cataclysmic variables	5
White dwarfs	5
Normal galaxies	6
Emission-line AGNs	45
BL Lac objects	11
Planetary nebulae	1
Unidentified	10

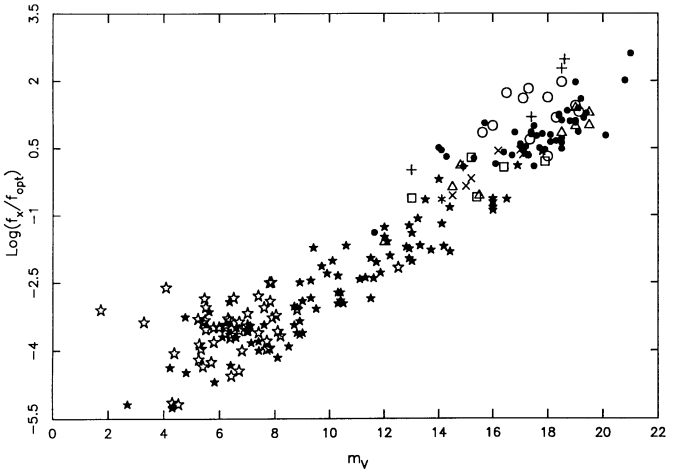

FIG. 3.—Plot of log (f_x/f_{opt}) vs. optical apparent magnitude for the 210 sources included in the HGLS complete sample (see text for definitions).

12. THE LOG N–LOG S RELATION OF ACTIVE GALACTIC NUCLEI

We consider here the subsample of all sources identified with active galactic nuclei and divide it into two subgroups: (1) emission-line AGNs and (2) BL Lac objects. In the following we derive the number-flux relation, or log N–log S of the emission-line AGN subgroup. The log N–log S of BL Lacs will be presented elsewhere (see Giommi et al. 1989 for a summary of the preliminary results).

Once the sky coverage of a survey is known, and the survey is statistically complete, the log N–log S of different classes of sources can be easily calculated. In order to compare our results with those of the *Einstein* EMSS (Gioia et al. 1990), fluxes were calculated in the 0.3–3.5 keV energy band and corrected for Galactic absorption (i.e., S is the flux before absorption by interstellar material in our Galaxy). Of the 10 objects in the sample that are still spectroscopically unidentified, seven show a F_x/F_{opt} ratio that is typical of AGNs. These sources have been used together with the 45 confirmed active galaxies to derive the log N–log S of AGNs.

Since the sky coverage of the HGLS is a strong function of the X-ray spectral slope α of extragalactic sources (see Fig. 1),

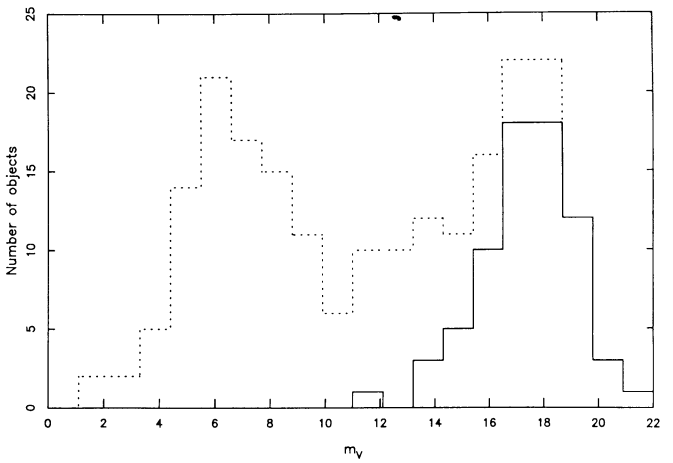

FIG. 4.—Apparent visual magnitude of all sources in the HGLS complete sample (*dotted histogram*) and of the extragalactic sources (*solid histogram*).

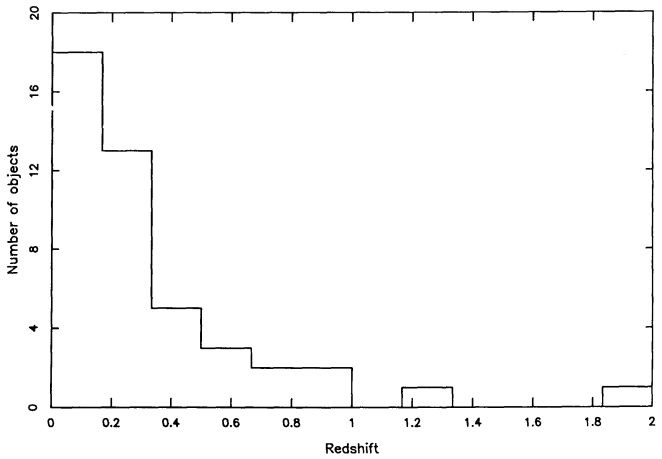

FIG. 5.—Redshift distribution of extragalactic sources in the HGLS

the derived log N–log S relationship will also strongly depend on α.

Given the relatively small number of objects in the sample and the strong dependence on α, we will not attempt to obtain a best-fit value for the log N–log S slope. Figure 6 shows the log N–log S of the subsample of emission-line AGNs for $\alpha = 0.7$ (*filled circles*), $\alpha = 1.5$ (*open circles*), and $\alpha = 2.5$ (*asterisks*). From Figure 6 we see that the *slope* of the log N–log S relation does not change much with α and is consistent with the Euclidean value of 1.5 for all the spectral slopes considered. The normalization of the log N–log S relation instead changes considerably with α. The dotted line shown in Figure 6 represents a power law with slope of 1.62, which is the latest best estimate of the log N–log S relation of AGNs obtained with EMSS data (I. M. Gioia et al. 1990, private communication). The case $\alpha = 1.5$ reproduces very well the EMSS results, while flatter slopes ($\alpha \leq 1.0$) or much steeper slopes clearly do not agree with the EMSS log N–log S.

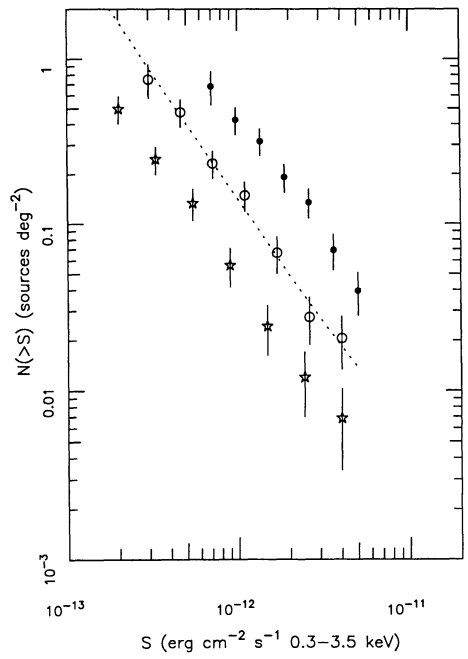

FIG. 6.—Log N–log S relationship of AGNs for three different assumptions of the AGN average energy spectral slope α. Filled circles are for $\alpha = 0.7$, open circles for $\alpha = 1.5$, and asterisks for $\alpha = 2.5$. The dotted line represents the log N–log S relation of AGNs estimated from *Einstein* EMSS data (I. M. Gioia et al. 1990, private communcation).

13. THE EFFECTS OF INTERSTELLAR ABSORPTION

We have seen in the previous section that a very steep spectral slope ($\alpha \sim 1.5$) is required if consistency between the *EXOSAT* and the EMSS log N–log S results is to be achieved. A second method of deriving information about α consists in studying the number of AGNs detected as a function of the amount of interstellar material, N_H, along the pointing direction of the fields considered (Giommi & Tagliaferri 1986; Giommi et al. 1988b; Zamorani et al. 1988). The system composed of the *EXOSAT* telescope and the CMA detector was sensitive in the very soft X-ray energy band, 0.05–2.0 keV, where the effects of absorption due to interstellar material are particularly important. This causes the CMA to preferentially detect extragalactic sources where the amount of N_H is low and the Galaxy is more transparent.

This effect is apparent in Figure 7, where the distribution of N_H along the pointing direction of each field, estimated from radio measurements (Stark et al. 1984 and Parkes data), is shown (*solid histogram*) together with the corresponding distribution for extragalactic serendipitous sources (*dotted histogram*). It is clear that extragalactic sources are mainly detected in fields where the amount of N_H is low. A Kolmogorov-Smirnov test rejects the hypothesis that the two distributions are the same with a confidence of 1×10^{-6}. The same test applied to the subsample of late-type stars, which are not expected to be correlated with N_H because of their very low intrinsic X-ray luminosity, and consequently small distance (Giommi et al. 1988b), finds that the two distributions are fully consistent with being identical ($P = 0.7$).

It can be easily shown that the expected number of AGN detections in different N_H bins is a function of the spectral slope α (Giommi et al. 1988b). Therefore, by comparing the fraction of AGNs detected in each N_H bin with that expected (assuming no intrinsic absorption), some additional information about α can be obtained. We have done this using the maximum-likelihood method described in Giommi et al. (1988b), and we

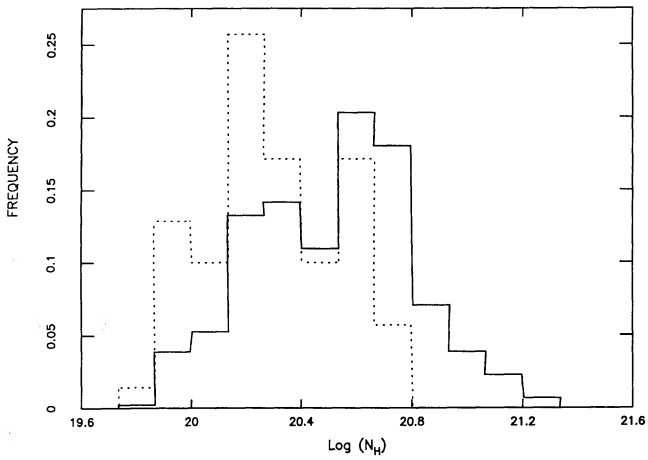

FIG. 7.—Distribution of the amount of interstellar material (N_H) along the pointing direction of all fields in the HGLS (*solid histogram*) and distribution of AGN detections as a function of N_H (*dotted histogram*).

have obtained a best-fit value of $\alpha = 1.45^{+0.35}_{-0.45}$. This is in very good agreement with the spectral slope implied by the comparison between the HGLS and the EMSS log N–log S.

14. DISCUSSION

In contrast to the remarkable uniformity seen at higher energies where the spectrum of most AGNs can be described by a simple power law with slope 0.7–0.8 (Mushotzky 1984; Turner & Pounds 1989), evidence for complex spectra in the soft X-ray band has been found in several AGNs using pointed data from both the *Einstein Observatory* and *EXOSAT* (Arnaud et al. 1985; Singh, Garmire, & Nousek 1985; Wilkes & Elvis 1987; Turner & Pounds 1989; Kruper, Urry, & Canizares 1990). In particular, a sharp steepening at low energies, commonly referred to as soft X-ray excess, has been detected in a number of objects. Soon after the launch of *EXOSAT*, the study of CMA serendipitous sources indicated that very steep energy spectra could be a frequent phenomenon in active galactic nuclei (Branduardi-Raymont et al. 1985). This result was, however, based on a very small number of objects and needed confirmation. This paper provides evidence, based on a much larger statistical sample, that a population of AGNs characterized by a steep soft X-ray spectrum and little intrinsic absorption indeed exists. The comparison between the log N–log S relation of AGNs derived from the HGLS and that obtained from the *Einstein* EMSS and the analysis of the N_H distribution of serendipitous AGN detections within the *EXOSAT* HGLS both imply that the average spectral slope of AGNs in the soft X-ray energy band is steep ($\alpha \approx 1.5$) and inconsistent with the canonical value of 0.7 seen in the hard X-ray band (Mushotzky 1984; Turner & Pounds 1989). An analysis of the distribution of the IPC hardness ratios of EMSS AGNs showed that $\alpha = 1.03 \pm 0.05$ with an intrinsic dispersion of $\sigma_\alpha = 0.36$ (Maccacaro et al. 1988). The difference between this value and that obtained with our data strongly indicates that the average spectral slope of AGNs steepens between the IPC (0.3–3.5 keV) and the CMA (0.05–2.0 keV) energy bands.

Recent results based on fluctuation analyses of hard X-ray data collected with the large area counter (LAC) (Turner et al. 1989) of the *Ginga* satellite, and with the A-2 experiment aboard the *HEAO 1* satellite, show that the normalization of the log N–log S relation of extragalactic sources in the hard X-ray energy band (2–10 keV) may be about a factor of 3 higher than that of the EMSS (Warwick & Stewart 1989; Lanczychi, Arnaud, & Mushotzky 1990). Reconciliation between the hard X-ray counts and the EMSS results can be obtained assuming that most of the extragalactic sources are heavily absorbed or assuming that their average energy spectral index is very flat ($\alpha \approx 0.4$; Warwick & Stewart 1989). Since the second case can be excluded by the results presented in this paper and by the hardness-ratio analysis of IPC serendipitous sources (Maccacaro et al. 1988), intrinsic absorption is left as the most likely explanation. Fluctuation analysis is, however, subject to uncertainties because of some important underlying assumptions, such as no intrinsic clustering of AGNs, and to the fact that the analysis performed is close to the limit of the instrumentation where systematic errors can be important. Confirmation of the hard X-ray results is therefore needed before any definite conclusion can be drawn. Precise measurements of the hard X-ray log N–log S relation of AGNs will be obtained by means of the surveys that can be performed using the imaging instruments of the SAX (Perola 1988), *Astro-D*, and *Jet-X* X-ray observatories that are sensitive in the $\approx$0.1–1 to 8–10 keV energy band.

The *Einstein* EMSS is a factor of 3–5 (depending on the spectral slope assumed) deeper than the *EXOSAT* HGLS and contains a factor of 8–9 ($\approx$400/45) more AGNs, which is consistent with the steep log N–log S of emission line AGNs. The detection ratio, however, reduces to only $\approx$3 ($\approx$34/11) when BL Lacs are considered, reflecting the deep difference in the number-counts relation of these two classes of objects that has been noted by, e.g., Maccacaro et al. (1984), Giommi et al. (1989), and Wolter et al. (1991).

All BL Lac objects in our sample have been detected at radio frequencies. This strengthens the conclusion of Stocke et al. (1990) that there is no evidence for a population of radio-quiet BL Lacs among X-ray sources.

Although on the basis of the EMSS we would expect about eight clusters of galaxies in the HGLS, none have been detected. This is due to the fact that, because of background limitations, the CMA detector was not sufficiently sensitive to low-brightness extended sources, and that the software used was optimized for the detection of pointlike objects. In addition, most bright clusters with intensity $S > 5 \times 10^{-12}$ ergs cm^{-2} s^{-1} were well-known X-ray emitters before the launch of *EXOSAT*, and several of them were chosen as targets of CMA observations. These clusters, therefore, could not be found as serendipitous sources, unless they happened to be included in the field of a nearby independent target, a condition that is rarely satisfied, since the HGLS only covers about 3% of the sky.

About 60% of the sources in our sample are stars, a much higher percentage than that found in the *Einstein* EMSS (25%). Many of these sources are early-type stars, most of which have been detected only because of a residual transparency to UV radiation of the thin Lexan filter. However, even considering late-type stars only ($\approx$36% of the sample), the percentage of stellar sources in the HGLS is significantly higher than that found in the *Einstein* EMSS.

Besides coronal emission main-sequence stars, several other Galactic objects were found. A remarkable difference between the HGLS and the EMSS is the detection rate of cataclysmic variables and white dwarfs. Despite the fact that the EMSS is much more effective in detecting extragalactic objects, the same number of cataclysmic variables (five) were detected in each survey, while five white dwarfs were found in the HGLS and only one in the EMSS. Such differences in the detection rate of Galactic sources were expected given the lower bandpass of the *EXOSAT* CMA and the softness of the energy spectrum of these objects. We expect that among the bright sources [$>(2–5) \times 10^{-13}$ ergs cm^{-2} s^{-1}] of the *ROSAT* sky survey the fraction of stars should be $\approx$40% or larger, and that a much higher percentage of cataclysmic variables and white dwarfs than that of the *Einstein* EMSS should be found.

The Calar Alto Observatory is operated by the Max-Planck-Institut für Astronomie, Heidelberg, jointly with the Spanish National Commission for Astronomy. The William Herschel and Isaac Newton telescopes, on the island of La Palma, are operated by the Royal Greenwich Observatory at the Spanish Observatorio del Roque de los Muchachos of the Instituto de Astrofísica de Canarias. K. O. M. acknowledges the support of the Royal Society and J. P. D. M. that of the SERC. We thank I. M. Gioia and the members of the *Einstein* EMSS team for providing an unpublished estimate of the EMSS log N–log S of active galactic nuclei, and A. Smale, J. Allington-Smith, and E. M. Puchnarewicz for assistance with optical observations.

REFERENCES

Arnaud, K. A., et al. 1985, MNRAS, 217, 105
Becker, R. H., White, R. L., & Edwards, A. L. 1991, ApJS, 75, 1
Beuermann, K. 1988, Adv. Space Res., 8, 292
Beuermann, K., Stella, L., & Sieber, W. 1984, in X-Ray and UV Emission from Active Galactic Nuclei, ed. W. Brinkmann & J. Trümper (Garching: MPE), 254
Beuermann, K., Thomas, H. C., Giommi, P., & Tagliaferri, G. 1987, A&A, 175, L9
Beuermann, K., Thomas, H.-C., Giommi, P., Tagliaferri, G., & Schwope, A. D. 1989, A&A, 219, L7
Beuermann, K., Thomas, H.-C., & Schwope, A. 1988, A&A, 195, L15
Beuermann, K., Thomas, H.-C., Schwope, A. D., Giommi, P., & Tagliaferri, G. 1990, A&A, 238, 187
Branduardi-Raymont, G., Mason, K. O., Murdin, P. G., & Martin, C. 1985, MNRAS, 216, 1043
Branduardi-Raymont, G., et al. 1989, in Proc. 23d ESLAB Symposium (ESA SP-296; Nordwijk: ESA), 2, 713
Caillault, J. P., Helfand, D. J., Nousek, J. A., & Takalo, L. O. 1986, ApJ, 304, 318
Chiappetti, L., & Giommi, P. 1985, The *EXOSAT* Express, 11, 37
Condon, J. J., Broderick, J. J., & Seielstad, G. A. 1989, AJ, 97, 1064
De Grijp, M. H. K., Miley, G. K., & Lub, J. 1987, A&AS, 70, 95
DeKorte, P. A. J., et al. 1981, Space Sci. Rev., 30, 495
Elvis, M., Plummer, D., & Fabbiano, G. 1990, in Proc. 23d ESLAB Symposium (ESA SP-296; Nordwijk: ESA), 2, 1111
Fleming, T. A., Gioia, I. M., & Maccacaro, T. 1989, ApJ, 340, 1011
Fleming, T. A., Liebert, J., Gioia, I. M., & Maccacaro, T. 1988, ApJ, 331, 958
Gioia, I. M., Maccacaro, T., Schild, R. E., Stocke, J. T., Liebert, J. W., Danziger, I. J., Kunth, D., & Lub, J. 1984, ApJ, 283, 495
Gioia, I. M., Maccacaro, T., Schild, R. E., Wolter, A., Stocke, J. T., Morris, S. L., & Danziger, I. J. 1986, in IAU Symposium 121, Observational Evidences of Activity of Galaxies, ed. E. Kachikian, G. Melnick, & K. Fricke (Byurakan: Byurakan Ap. Obs.)
Gioia, I. M., Maccacaro, T., Schild, R. E., Wolter, A., Stocke, J. T., Morris, S. L., & Henry, J. P. 1990, ApJS, 72, 567
Giommi, P. 1985, The *EXOSAT* Express, No. 12, p. 33
Giommi, P., & Angelini, L. 1987, The *EXOSAT* Express, No. 18, p. 45
Giommi, P., et al. 1988a, BAAS, 20, 1035
Giommi, P., & Tagliaferri, G. 1986, in IAU Symposium 124, Observational Cosmology, ed. A. Hewitt, G. Burbidge, & L. Fang (Dordrecht: Reidel), 601
Giommi, P., Tagliaferri, G., & Angelini, L. 1988b, in X-Ray Astronomy with *EXOSAT*, ed. N. E. White & R. Pallavicini (Mem. Soc. Astr. Italiana, 59, 33)
Giommi, P., et al. 1989, in Proc. Workshop on BL Lac Objects, ed. L. Maraschi, T. Maccacaro, & M.-H. Ulrich (Berlin: Springer-Verlag), 231
Giommi, P., Tagliaferri, G., Branduardi-Raymont, G., & Beuermann, K. 1991, in preparation
Halpern, J. P., Impey, C. D., Bothun, G. D., Tapia, S., Schillman, E. D., Wilson, A. S., & Meurs, E. J. A. 1986, ApJ, 302, 711
Hewitt, A., & Burbidge, G. 1987, ApJS, 63, 1
Hoffleit, D., & Jaschek, C. 1982, The Bright Star Catalogue (4th ed.; New Haven: Yale Univ. Obs.)
Johnston, K. J., Biermann, P., Eckart, A., Kühr, H., Strittmatter, P. A., Strom, G., Witzel, A., & Zenzus, A. 1984, ApJ, 280, 542
Kruper, J. S., Urry, C. M., & Canizares, C. R. 1990, ApJS, 74, 347
Lanczychi, C., Arnaud, K., & Mushotzky, R. 1990, GSFC internal report
Maccacaro, T., et al. 1982, ApJ, 253, 504
Maccacaro, T., Gioia, I. M., Maccagni, D., & Stocke, J. T. 1984, ApJ, 284, L23
Maccacaro, T., Gioia, I. M., Wolter, A., Zamorani, G., & Stocke, J. T. 1988, ApJ, 326, 680
Maccacaro, T., Romaine, S., & Schmitt, J. 1986, in IAU Symposium 124, Observational Cosmology, ed. A. Hewitt, G. Burbidge, & L. Fang (Dordrecht: Reidel), 597
Margon, B., Downes, R. A., & Chanan, G. A. 1985, ApJS, 59, 23
Mewe, R., Gronenschild, E. H. B. M., & Van den Oord, G. H. J. 1985, A&AS, 62, 197
Mittaz, J. P. D., et al. 1991, in preparation
Mushotzky, R. F. 1984, Adv. Space Res., 3, 10
Osborne, J. 1991, The *EXOSAT* Express, No. 19, in press
Osborne, J., Giommi, P., Angelini, L., Tagliaferri, G., & Stella, L. 1988, ApJ, 328, L45
Pallavicini, R., Monsignori-Fossi, B. C., Landini, M., & Schmitt, J. H. 1988, A&A, 191, 109
Perola, G. C. 1988, in Hot Thin Plasma in Astrophysics, ed. R. Pallavicini (Dordrecht: Kluwer), 369
Reichert, G. A., Mason, K. A., Thorstensen, J. R., & Bowyer, S. 1982, ApJ, 260, 437
Singh, K. P., Garmire, G. P., & Nousek, J. A. 1985, ApJ, 297, 633
Stark, A., Heiles, C., Baily, J., & Linke, R. 1984, privately distributed tape
Stocke, J. T., Liebert, J., Gioia, I. M., Griffiths, R. E., Maccacaro, T., Danziger, I. J., Kunth, D., & Lub, J. 1983, ApJ, 273, 458
Stocke, J. T., Morris, S. L., Gioia, I. M., Maccacaro, T., Schild, R. E., & Wolter, A. 1990, ApJ, 348, 141
Stocke, J. T., Morriz, S. L., Gioia, I. M., Maccacaro, T., Schild, R., Wolter, A., Fleming, T. A., & Henry, J. P. 1991, ApJS, 76, 813
Tagliaferri, G., Doyle, J. G., & Giommi, P. 1990, A&A, 231, 131
Tagliaferri, G., Giommi, P., Angelini, L., Osborne, J. P., & Pallavicini, R. 1988, ApJ, 331, L113
Taylor, B. G., Andresen, R. D., Peacock, A., & Zobl, R. 1981, Space Sci. Rev., 30, 479
Thomas, H.-C., Beuermann, K., Graser, U., Giommi, P., & Tagliaferri, G. 1991, in preparation
Trümper, J. 1984, in X-Ray and UV Emission from Active Galactic Nuclei, ed. W. Brinkmann and J. Trümper (Garching: MPE), 254
Trümper, J., 1983, Adv. Space Res., 2 (No. 4), 241
Turner, M. J. L., et al. 1989, PASJ, 41, 345
Turner, T. J., & Pounds, K. A. 1989, MNRAS, 240, 833
Véron-Cetty, M. P., & Véron, P. 1989, ESO Sci. Rept., No. 7
Warwick, R. S., & Stewart, G. C. 1989, in Proc. 23d ESLAB Symposium (ESA SP-296; Noordwijk: ESA), 727
White, N. E., & Giommi, P. 1990, in Database and On-Line Data in Astronomy, ed. D. Egret & M. Albrecht, in press
White, N. E., & Peacock, A. 1988, in X-Ray Astronomy with *EXOSAT*, ed. N. E. White & R. Pallavicini (Mem. Soc. Astr. Italiana, 59, 7)
Wilkes, B., & Elvis, M. 1987, ApJ, 323, 243
Wolter, A., Gioia, I. M., Maccacaro, T., Morris, S. L., & Stocke, J. T. 1991, ApJ, 369, 314
Zamorani, G., Gioia, I. M., Maccacaro, T., & Wolter, A. 1988, A&A, 196, 39